Upstream Blockage and Downstream Wake Flow of a Wind Turbine

Runar Garnes

Jan W Jensen

Andreas Rogne

Bachelor's thesis in Energy Technology

Bergen, Norway 2020

Høgskulen på Vestlandet

Upstream Blockage and Downstream Wake Flow of a Wind Turbine

Runar Garnes

Jan W Jensen

Andreas Rogne

Department of Mechanical- and Marine Engineering

Western Norway University of Applied Sciences

NO-5063 Bergen, Norway

IMM [2020]-M[17]

Høgskulen på Vestlandet

Fakultet for Ingeniør- og Naturvitskap

Institutt for maskin- og marinfag

Inndalsveien 28

NO-5063 Bergen, Norge

Norsk tittel:	Oppstrøms Blokkasje og Nedstrøms Vake for en Vindturbin
Author(s), student number:	Runar Garnes, 132916
	Jan William Jensen, 572018
	Andreas Rogne, 571998
Study program:	Energy Technology
Date:	05.2020
Report number:	IMM 2020-M71
Supervisor at HVL:	Jan Bartl
Assigned by:	HVL, co-supervised by Equinor ASA
Contact person:	Marte Godvik
Antall filer levert digitalt:	1/1

Preface

This thesis is written as part of the Bachelor program in Energy Technology at the Department of Mechanical and Marine Engineering at Western Norway University of Applied Sciences (WNUAS). The Supervisors for this thesis are Jan Bartl and Marte Godvik (Equinor ASA and University of Bergen).

We will start of with sincerely expressing our gratitude to our supervisor Jan Bartl for his advice, guidance, and support throughout this thesis writing. By sharing his exceptional knowledge and commitment far beyond all expectations we are forever thankful. We would also like to thank HVL for allowing us to use Marin Lab and the equipment needed to complete the experiment.

Acquiring knowledge on the wake effects around a wind turbine and how this influence the performance of a wind park is a subject we expect to be more and more relevant in the future, and so working on this project have given us a great personal gain, and an edge in terms of knowledge on the field and valuable experience in report writing and experimental techniques.

Also, we would like to express our gratitude to our families and friends for the love and support while completing this bachelor program, it has been a journey.

Abstract

In recent times there has been new discoveries on blockage and wake effects surrounding wind turbines, which are known to cause losses in power and increased fatigue loads. In this thesis blockage and wake flow measurements are performed in front and behind a porous disc made from aluminium in the towing tank at HVL's Marin Lab. The wake flow results are compared to previous results behind the same disc geometry measured at the wind tunnel laboratory at NTNU. Furthermore, profiles at -1D, 1D, 3D, 4D and 10D are compared to Jensen Gaussian Wake Model. The actuator disc representing a wind turbine's rotor is mounted on the towing carriage in certain distances to an Acoustic Doppler Velocimeter probe that can be adjusted by a traverse mechanism. The streamwise distance was adjusted from -1 to 10 rotor diameters and transverse velocity profiles and centerline velocities were measured upstream and downstream of the actuator disc. Results show that the wake has a Gaussian shape and a negative centerline velocity up until 2,4D. The wake recovers to 92% of the inflow velocity at 10D, while turbulence kinetic energy in the wake decays by 72,7% from 1D to 10 D

A comparison of measurements behind the same disc geometry with wind tunnel results from NTNU shows that air tunnel and water tank experiments are consistent with each other. The profile results are also compared with the Jensen Gaussian Wake Model at 1D, 3D, 4D and 10D, confirming the weakness of this engineering wake model to predict wake results in a low-inlet turbulence environment. The upstream centerline velocity reduction is compared with Biot-Savart-Law, which is shown to underestimate the velocity reduction at the given thrust coefficient. This thesis concludes, based on the results, that the Marin Lab's water tank is suitable for model-scale-wake and blockage flow experiments of wind turbines.

Sammendrag

I fjor oppdaget man nye funn rundt blokkeringeffekter og waker på vindturbiner, som reduserer energiproduksjonen og øker utmattelseslaster. I denne oppgaven utføres målinger av "wakes" foran og bak en porøs disk laget av aluminium i slepetanken ved HVL's Marin Lab. Målingsresultatene sammenlignes med tidligere måleresultater bak en disk med samme geometi utført i vindtunnelen ved NTNU. Videre sammenlignes profiler på -1D, 1D, 3D, 4D og 10D med Jensen Gauss Wake modellen. Aktuatorskiven som representerer en vindturbin er montert på slepevognen i visse avstander til en akustisk Doppler Velocimeter som kan justeres ved hjelp av en traversmekanisme. Nedstøms avstanden ble justert fra -1 til 10 rotordiameter og tverrsnittsprofiler/senterlinjer ble målt for hastigheten både oppstrøms og nedstrøms. Resultatene viser at vaken har en gaussform og at hastigheten er negativ opp til 2,4D. Vaken henter seg inn igjen til 92% av innløpshastigheten på 10D, mens den turbulente kinetiske energien i vaken reduseres fra med 72,7% fra 1D til 10D

En sammenligning av målingene bak samme skivegeometri med vindtunnel-resultater fra NTNU viser at eksperimentene i vindtunnel og vanntank stemmer overens med hverandre. Profil-resultatene blir også sammenlignet med Jensen Gauss Wake Modellen ved 1D, 3D, 4D og 10D, og bekrefter svakheten ved denne tekniske vake-modellen for å forutsi vaker i et miljø med lite innløpsturbulens. Senterlinjen på oppstrømsmålingene sammenlignes med Biot-Savart-Law, og viser seg å undervurdere hastighetsreduksjonen ved den gitte Thrust koeffisienten. Denne oppgaven konkluderer med, basert på resultatene, at Marin Laben ser ut til å være egnet for både vake- og blokkeringseksperimenter for vindturbiner.

Table of contents

1. Introduction

Renewable energy is expected to play a major role in meeting future energy needs while mitigating climate change and environmental pollution. While world energy demand continues to increase in an annual rate of 2%, most of that demand (around 80%) is being met by fossil fuels (IEA2018), with the well-known negative impacts on the environment and climate. This, together with the growing concerns surrounding nuclear energy, many countries have set ambitious strategic targets for renewable energies with low greenhouse gas and pollutant emissions, including wind energy [1]. Long term sustainable development of wind energy requires knowledge on how wake effects influence the overall efficiency and energy output of a wind farm. Over the last decades both size and quantity of turbines in windfarms has increased rapidly, and it is getting more and more important to understand the interactions between single turbines in a windfarm to further improve the overall performance.

A wake is created as front row turbines extract energy from the incoming wind which creates a velocity deficit and increased turbulence, and this becomes the inlet condition of the back-row turbines, and the goal is to minimize these losses [2]. Since the seminal work of Betz (1920) and Joukowsky (1920), substantial research efforts have been made in the field of wind-turbine aerodynamics, and particulary in the optimization of horizontal-axis wind turbines (HAWT) rotors. Many theories which have been extended with many “engineering rules” have been developed over the years, but the predictions of the turbine’s performance under real conditions remains an elusive target and one of the main challenges in optimizing the layout, operation and control of wind farms. This due to the complex interactions between wind turbines and the atmospheric boundary layer (ABL) which is highly turbulent and non-stationary [1].

As recent as in October 2019, Danish wind developer, Ørsted announced that it had revised its estimates for future energy production of its offshore wind farms as a result of improving its methodology for calculating turbine interaction loss, i.e the amount by which energy production by a wind farm turbine declines due to the presence of the other wind farm turbines. By using field measurements and simulation results, it showed that blockage effects cause wind speed reductions upstream of a wind farm that are more pronounced and far-reaching than commonly assumed. Turbine interaction models used by the industry to estimate future wind farm energy yield, have not typically accounted for this blockage effect. Therefore, it is likely that turbine interaction losses have been underestimated across the industry. [3]

The present report’s purpose is to quantify the upstream and downstream flow of a pourous actuator disc in the zero-turbulence environment of a towing tank. The results are furthermore used to validate wake models based on experiments performed in the Marin Lab at Western Norway Univeristy of Applied Science.

2. Theory

A wind turbine extracts mechanical energy from the kinetic energy of the wind. It is useful to examine a simple one-dimensional (1-D) model of an idealized rotor as a non-rotation actuator disc. This simplification allows us to understand the large-scale flow effects upstream (blockage region) and wake region of the rotor disc without taking rotational effects or tip vortex effects into account.

2.1 Actuator Disc

The permeable disc simulates a rotor and is considered ideal; in other words, it is frictionless and there is no rotational velocity component in the wake. The actuator disc acts as a drag device slowing the water speed from V_0 far upstream of the rotor to u at the rotor plane and to u_1 in the wake. Therefore, the streamlines must diverge as shown in figure 1. The drag is obtained by a pressure drop over the rotor. Using the assumptions of an ideal rotor it is possible to derive simple relationships between the velocities V_0, u_1 and u, the thrust T, and the absorbed shaft power P. The thrust is the force in the streamwise direction resulting from the pressure drop over the rotor, and is used to reduce the wind speed from V_0 to u_1:

$$\boldsymbol{T = \Delta p A}$$

Where $A = \pi R^2$ is the area of the rotor. The flow is stationary, incompressible and frictionless and no external force acts on the fluid up- or downstream of the rotor. [4]

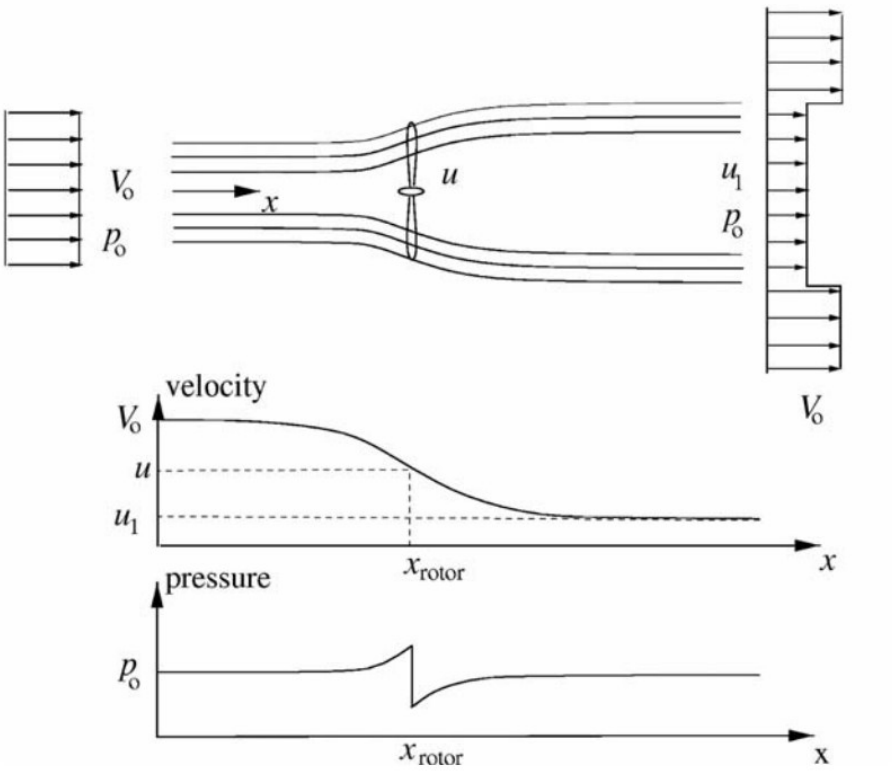

Figure 2.1 Circular control volume around a wind turbine [4].

As shown in the figure above, the magnitude of the change in the velocity around the wind turbine is often measured using the induction factor, ***a.*** which changes along the length of the blade and also the air flow downstream of the rotor during the operation. [5] For an actuator disc (ideal rotor) there is no rotation in the wake; in other words, the rotational induction factor is zero. The flow is assumed to be frictionless and therefore there is no change in the internal energy from the inlet to the outlet of the streamline. The shaft power P can be found using the integral energy equation on the control volume shown in figure 2.2:

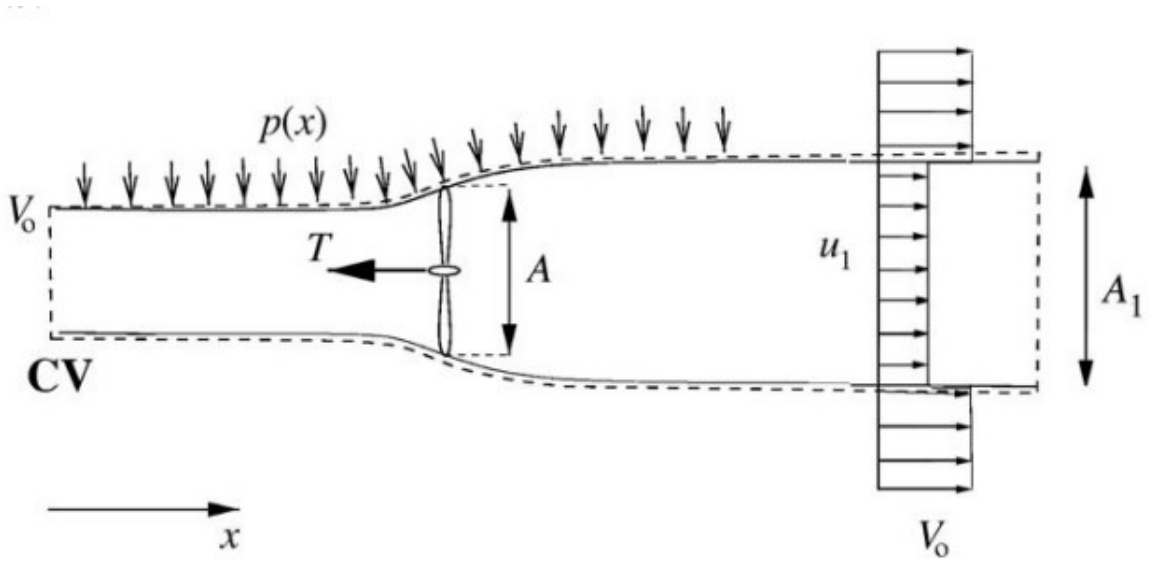

Figure 2.2 Control volume around a wind turbine [4].

The axial induction factor **a** is defined as (derivation of this formula can be found in Hansen [4]) :

$$u = (1 - 2\boldsymbol{a})V_0$$

And the thrust coefficient C_T can be described as:

$$C_T = 4\boldsymbol{a}(1 - \boldsymbol{a})^2$$

This thrust coefficient C_T is an important dimensionless number in aerodynamics and describes the axial forces on the rotor or actuator disc. The induction factor describes the ratio of speed reduction the flow

passing through the rotor plane has relatively to the far upstream velocity of the turbine. Experiments have shown that the assumptions of an ideal wind turbine are only valid for an axial induction factor, **a**, of less than approximately 0.4. If the momentum theory were valid for higher values of **a,** the velocity in the wake would become negative as shown in equation above. For a wind turbine, a high thrust coefficient C_T, and thus a high axial induction factor a, is present at low wind speeds. The reason that the simple momentum theory is not valid for values of **a** greater than approximately 0.4 is that the free share layer at the edge of the wake becomes unstable when the velocity jump $V_o - u_1$ becomes too high and eddies are formed which transport momentum from the outer flow into the wake. This situation is called the turbulent -wake state, see figure below. [4]

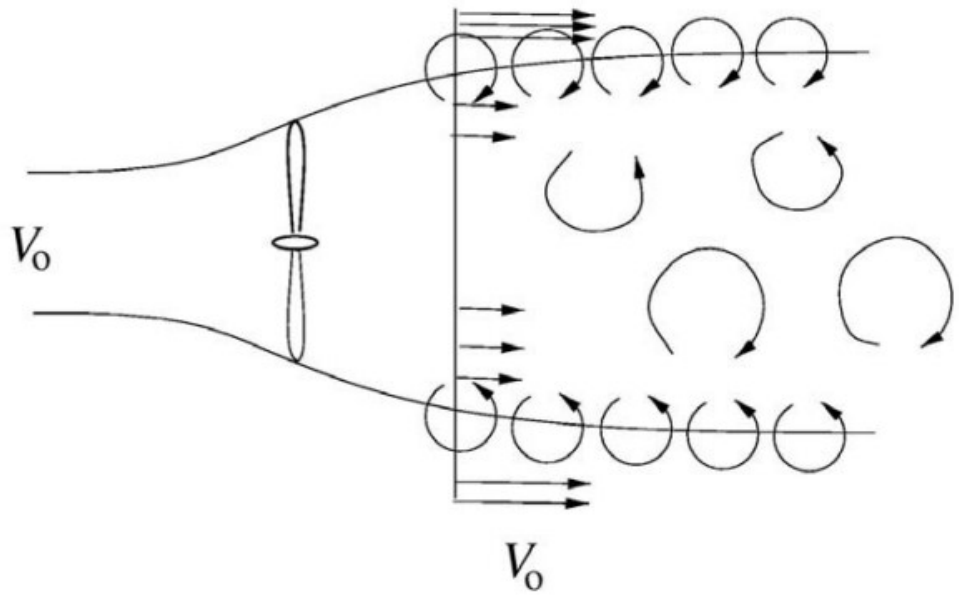

Figure 2.3 Schematic view of the turbulent-wake state induced by the unstable shear flow at the edge of the wake [4].

In terms of this issue there is a big advantage doing the experiments in water as you can go at lower speeds and keep a high Reynolds Number. At the certain Reynolds number, you can maintain the same thrust coefficient C_T and induction factor **a**.

Solving ***a*** in terms of the thrust coefficient yields this solution:

$$\boldsymbol{a} = \frac{1}{2} - \frac{1}{2}\sqrt{1 - C_T}$$

Recall that the axial induction factor, **a,** is defined as the ratio of the axial component of induced velocity at the turbine disc to the free stream velocity. The thrust coefficient of the present disc geometry has been previously measured to be $C_T = 0.82$ [Karlsen, NTNU] and putting that into the equation above we get an axial induced factor ***a*** = 0.29, which will be used in the experiment.

For upstream measurements Biot-Savart law makes it possible to obtain the flowing expression of the velocity U along the symmetry axis upstream of the actuator disc [6], and is applied to compare our experiment results upstream of the disc:

$$\frac{U}{U_0} = 1 - a[1 + \varepsilon(1 + \varepsilon^2)^{-0.5}]$$

Where U_0 is the undisturbed velocity, and $\varepsilon = x/R$, where x is the coordinate along the symmetry axis and R is the rotor radius. The current practice for power curve measurements assumes the influence on the flow speed in steady flow conditions by a turbine to be negligible at 2D upstream the rotor plane. Any change in the reference upstream flow speed can have important consequences on the estimate of the power coefficient of a turbine.

2.2 Wake Flow

Turbulence is created from the friction between two surfaces and wakes are generated from this friction. A flow can also have different amounts of turbulence before making contact with an object, which is called intake turbulence. The turbulence created by friction is added on top of the intake turbulence, often called rotor-added-turbulence. There is also rotation added to the wake from the blades spinning and tip vortices. The actuator disc will not generate a rotation in the wake as it is stationary. As the air travels downstream the surrounding freestream flow mixes with the wake and the wind recovers its velocity and energy.

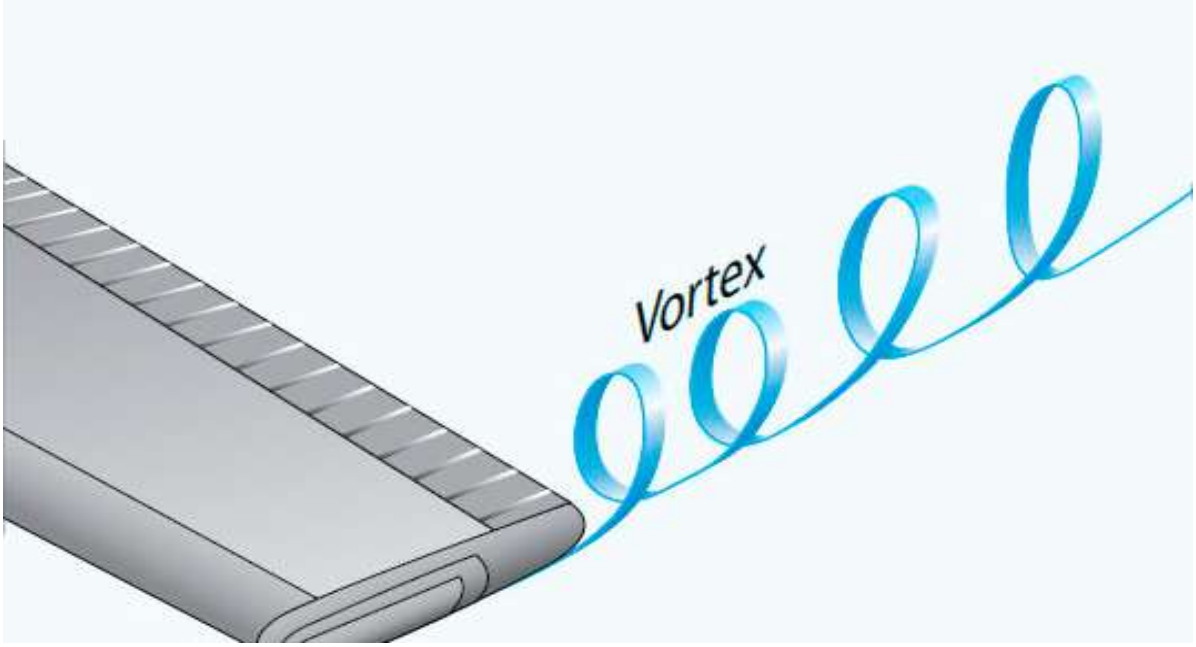

Figure 2.4 Wing tip vortex. [7]

In most experiments air is used as medium to test far wakes and turbulence on wind turbines. In some cases, however, water is used as the medium, which means the Reynolds number will be different from other experiments where air is used. Amongst others, Okulov et al. did an experiment in a water flume with a model of a model-scale wind turbine rotor and showed that it is possible to perform wake experiments in water. [7]

Wake models have been around for a long time and has been tested under lab conditions which have unified test results with numerical predictions. The predictions of real conditions on wind farms is far more complex with interactions between wind turbines and the atmospheric boundary layer which simulations can't yet achieve [8].

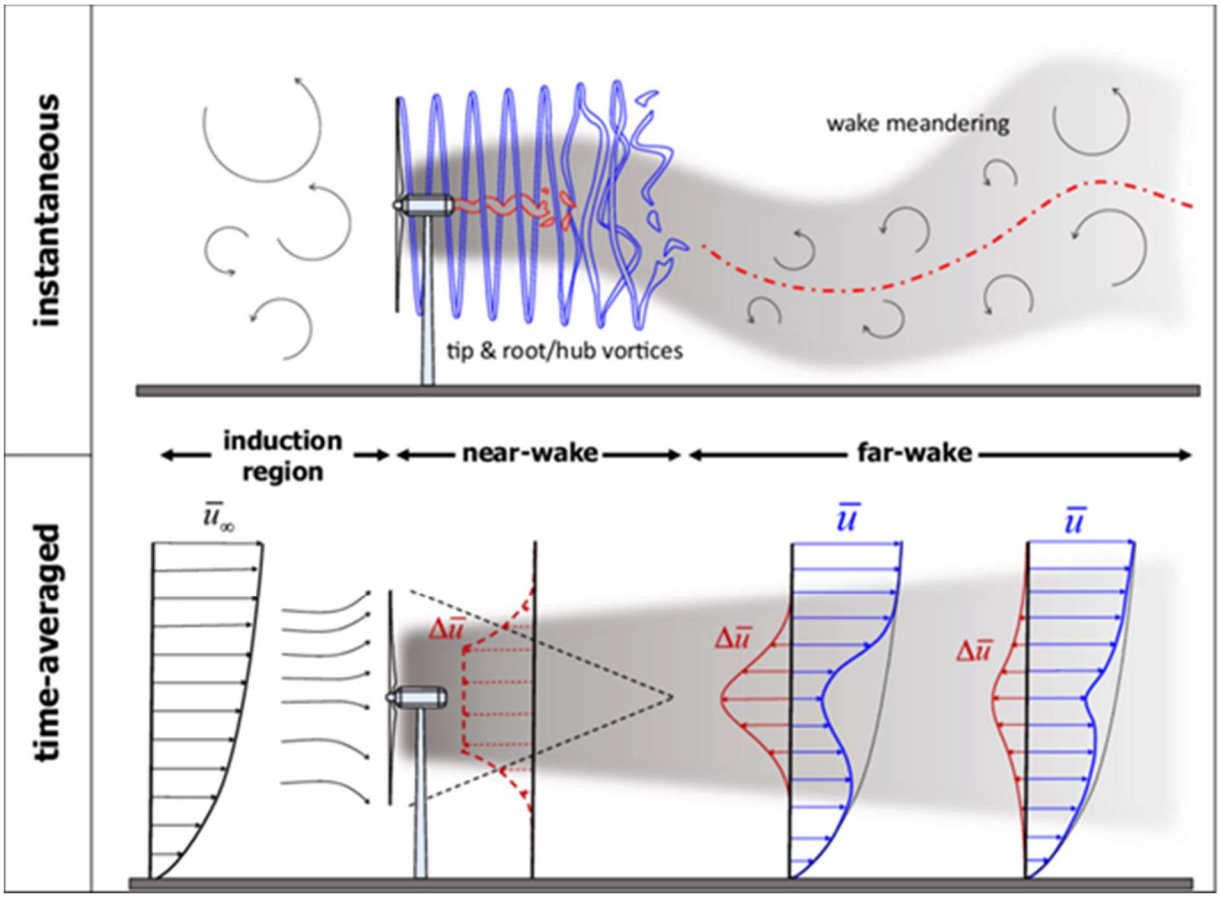

Figure 2.5 Wakes real time and averaged over time. [10]

There is plenty of models that try and predict these wakes. The Jensen model, developed in the 80s, which is a kinematic model with linear wake expansions. The Larsen model, from 1988, uses the Prandtl's turbulent boundary layer equation for flow calculation. The Frandsen model, from 2006, which is used for larger scarce wind farms configured in a grid pattern. There are many more, but these three models were compared in a studie by Liu and Gao in 2018 [9]. In this thesis the Jensen-Gaussian wake model is compared with experimental data. The Jensen-Katic model assumes that there is a top hat shape and has shown that there are inaccuracies between measured data and the preditions. The Jensen-

Gaussian model tries to correct these inaccuracies by including a second dimension. Where Jensen-Katic model only varies from the distance downstream, Jensen-Gaussian also considers the offset. The velocity deficit that comes with offset has the shape of a Gaussian distribution [10] [11]

A wake can be divided up into two sections: Near wake and far wake. The near wake is usually just reffered to as wake where there is turbulence generation. In the far wake there is mixing of flow that passed through the wind turbine and the surrounding air that goes around it, increasing the velocity of the flow back up to its original speed.

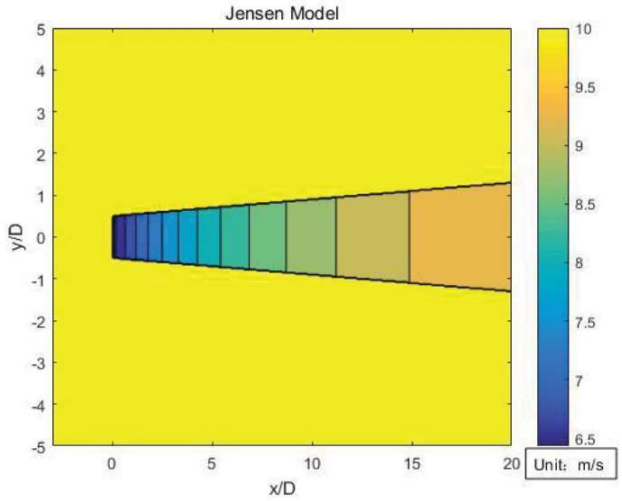

Figure 2.6 Jensen Wake Model. [39]

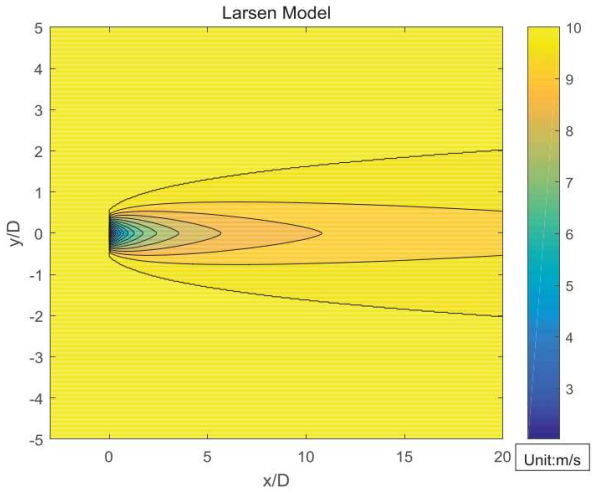

Figure 2.7 Larsen Wake Model. [39]

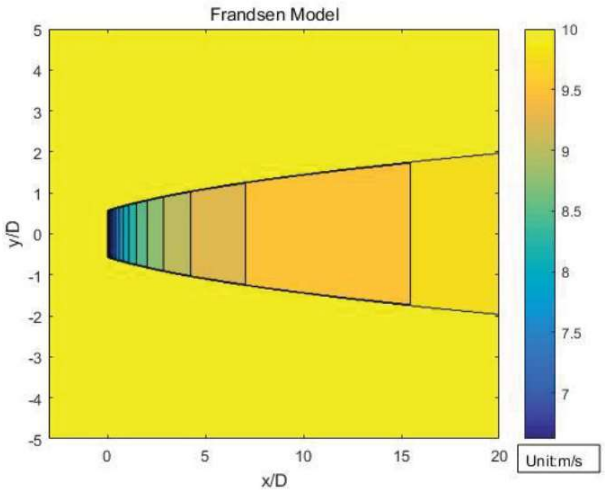

Figure 2.8 Frandsen Wake Model. [39]

2.3 Upstream Blockage

Most models that calculate interactions between wind farm turbines only consider wake effects. This assumption is called the "wakes-only" approach. It is only recent that blockage effect has been considered as an interaction that can affect the energy output of wind farms. When the airflow is confined the blockage effect can increase the power output of a wind turbine, shown in a studie by Garrett and Cummins [12] where the pressure upstream is increasing power output above Betz limit:

$$C_p = \frac{P}{\frac{1}{2}\mathrm{r}\,\mathrm{U}_0^3 A}$$

Where ρ is the fluid density, U_0 is the upstream flow velocity and A is the disc area, the maximum power coefficient $C_{p\,max}$ is shown to be 16/27. When the blockage effect is considered, power output can exceed this limit if the local pressure upstream is higher than downstream.

$$\frac{16}{27} * (1 - BF)^{-2}$$

$$\mathrm{BF} = \frac{\mathrm{U}_0}{U}$$

Where BF is Blockage Factor, U_0 is the free stream wind speed and U is the wind speed at the rotor.

The blockage effect is larger for a windfarm than the sum of the same amounts of wind turbines' individual blockage effect. This blockage effect accounts for a loss from 0 to 4% of mean annual energy in a wind farm [3]. When looking at the blockage effect there is conflicting evidence where there are arguments that the blockage effect increases the power output of wind farms [13]. There is speculation that the increase in output power is due to local pressure differences, but it is evident that more reasearch is needed to understand this phenomenon in the wind energy sector. [14]

An article by Nishino and Willden [15] from 2012 a new theoretical model is proposed to explore the efficiency of tidal turbines in a long array to partially block the channel cross section. The model suggests that an optimal spacing of turbines exists where the turbines block the upstream flow enough to create a local blockage. If the turbines are placed too close to each other the flow through the entire array is reduced and a local blockage happens in front of the array. Even though the array has reduced flow the turbines can surpass Betz' limit of 0,593. When the local blockage gets increased a new limit is introduced which is 0,798. Increasing the local blockage further will decrease the efficiency. While the efficiency goes up, the velocity through the array goes down. Since the model is tested in tidal turbines a question arises: How can this model be applied to the setup of future wind parks? At what efficiency will most amount of kinetic energy be converted to electricity over time?

2.4 Scaling

The question may be asked to which degree an experiment with an Actuator disc in water can represent a full-scale wind turbine operated in the atmospheric boundary layer. To be able to determine the proper properties of the model it is necessary to develop scaling laws that ensures a similar behaviour of the Actuator disc in water and a real wind turbine in full scale. To achieve similarity in forces between the model scale and a full-scale situation geometrical scaling and scaling in terms of Reynolds number is discussed.

First, it must be mentioned that the representation of a three-bladed horizontal axis wind turbine as a disc is strongly simplified. However, when neglecting rotational effects induced by the rotor, the wake flow can be regarded as similar. Secondly, the experiment is executed in water instead of air. The main difference between water and air is the density and viscosity which allows us to reach higher values of Reynolds number at lower velocities. Scaling laws as discussed below, however, allow for conducting aerodynamic experiments in water under certain limitations. These limitations are primarily a change in hydrostatic pressure with depth and a free water surface which can transport pressure energy in the shape of waves.

The shape between the model disc and a full-scale wind turbine are geometrically similar, and it exists a constant diameter scale between them.

$$\alpha = \frac{D_{fs}}{D_{ms}}$$

Where D_{fs} and D_{ms} are any dimension of the full-scale turbine and model scale disc. The requirement to equal diameter ratio for all dimensions does not apply only to structures, but also to the surrounding environment. In the Marina Lab we have some uncertainties in terms on environment because the size of the tank itself and the water surface will affect the pressure distribution of the flow around the disc.

Modern wind turbines have a full-scale diameter up to D_{fs} = 200m [16], while the model disc diameter is D_{ms} = 0.20m. This results in a scaling ratio alpha = 1000.

Reynolds number is a dynamic similarity and is achieved if we have the same ratio at model scale and full scale for the different force contributions present in the problem. Reynolds Number is the ratio of inertial forces to viscous forces, and a dimensionless number used to categorize the fluids systems in which the effect of viscosity is important controlling the velocities or the flow pattern of a fluid and defined as:

$$Re = \frac{\rho v d}{\mu}$$

Where ρ is the fluid density, v is velocity, d is the disc diameter and μ is the viscosity. Since the experiment is performed in water the density is much higher than air, at the same time the viscosity counter some of this effect. Because of this ratio we can run lower velocities in water and achieve the same Reynolds Number as air on higher velocities. [17]

The Reynolds number in air for the full-scale turbine and in water for the model scaled disc can be calculated as:

$$Re_{fs} = \frac{1.225\frac{kg}{m^3} * 10\frac{m}{s} * 200m}{1.825 * 10^{-5}\ cP} \approx 13.4 * 10^7$$

$$Re_{ms} = \frac{1000\frac{kg}{m^3} * 0.5\frac{m}{s} * 0.2m}{1.0 * 10^{-3} cP} = 100{,}000$$

There is a big difference in the Reynolds numbers due to the differences in diameter, but this parameter is not possible to change under these circumstances. The density of air at 20 degrees is approximately 890 times smaller than the density of water, and the viscosity of air is around 55 times lower than water [18]. In air the relationship density/viscosity is approximately 15 times smaller than the same relationship for water, so therefore you can go with lower velocities in water and get the same Reynolds number.

3. Methodology

All the experiments were conducted at Marine Lab at HVL, in Bergen, Norway. Trough experimental methods data is collected from the experiments to assess theoretical knowledge. All good research depends on being able to reliably infer that things are related in the ways a theory thought they would be, or to understand what part of the predicted experimental results that needs revision.

3.1 Marin Lab

The testing equipment was mounted on a carriage that could move at a controlled velocity in both direction of a water tank. The tank has the following specifications: length of 50 m, width is 3 m and depth are 2,2 m. The velocity measurements as described in Section 3.1.3 require seeding powder in the water. This powder was mixed into the tank and a wave generator was used to help mixing. The actuator disc itself was also used to help with mixing by running the carriage through the tank for 5 to 10 minutes before testing. The carriage is constructed of aluflex material where both the actuator disc and the traverse mechanism for the velocity measurement are mounted. During the experiment, the carriage ran for 35 meters.

Since the experiment equipment was installed by hand to the carriage there is always the possibility for errors. The actuator disc and the Acoustic Doppler Velocimeter (ADV) was lined up to be vertical with with a spirit level. Once the equipment was angled right it was locked with bolts. The distance between the non-rotating actuator disc model (ADM-NR) and the ADV was measured both from center of disc to ADV and from installation point on the carriage.

Figure 3.1 Towing carriage above the water tank at HVL`s Marin Lab.

3.1.1 Actuator Disc Model-non-Rotational (ADM-NR)

The actuator disc was mounted to a thin circular rod with a diameter of 1 cm. The rod itself was mounted to the carriage with a connecting piece to the aluflex. The actuator disc needed to be perpendicular to the surface of the water and facing the direction of movement. It is important that the disc and all the other equipment is adjusted correctly within a margin of +/- 0.1° to ensure that the wake is axisymmetric. The rod was grinded down to have a flat surface so the contact point between the disc and rod do not allow the disc to rotate when moving while running the experiments. There is still the possibility for some inaccuracies with the rotation of the disc that was checked with a spirit level.

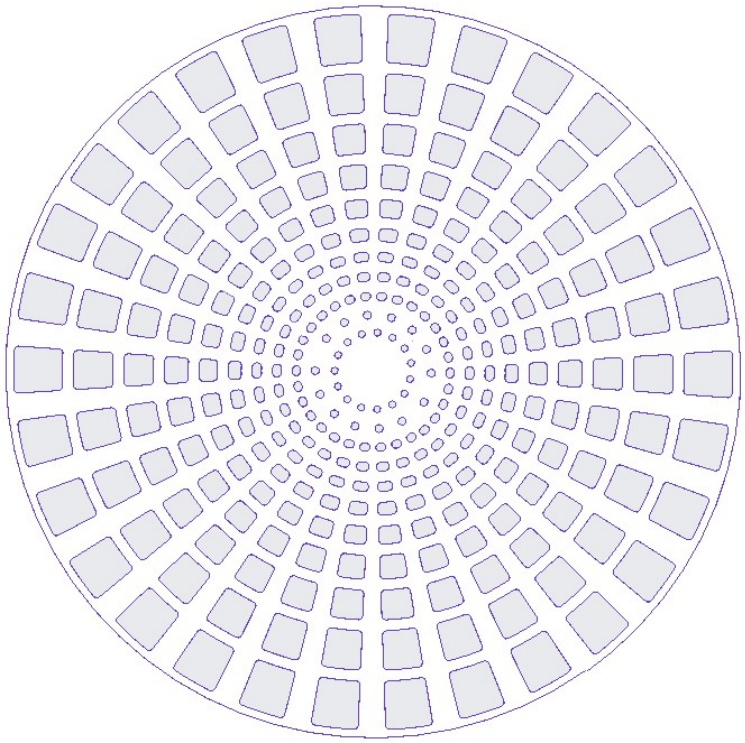

Figure 3.2 Actuator disc.

3.1.2 Flow measurements ADV

The velocity measurements were conducted using an Accoustic Doppler Velocimeter (ADV), of the type Vectrino Plus manufactured by Nortek. This is a high-resolution velocimeter used to measure 3D water velocity fluctuations with a rate of up to 200Hz. It consists of 4 reciever arms and one standard downwardslooking probe. [19]

Figure 3.3 Picture of the ADV used in the experiment. [39]

The Vectrino utilizes the doppler effect in order to measure velocity. The instrument sends out a short pulse of sound with constant frequency, listens to its echo and measures the change in frequency. This change in frequency is proportional to the velocity. However, the emitted sound pulse does not reflect from the water itself, but from small suspended particles. For this experiment these particles were distributed by hand. In order to get clean and good measurements, this distribution, called seeding, needs to be evenly distributed and sufficiently cover the ADV`s path.

For the Vectrino, there are mainly two sources of error, the seeding, which is done by hand, and electronical interference. An effort was made during the experiment to ensure that these errors became as insignificant as possible. The wires were kept as seperate as possible, and the seeding was executed carefully. In addition, the results were thoroughly analyzed with MatLab. This will be further explained in the next sub-chapter.

The ADV was connected to a traverse rig, which was constructed for the experiment, and others like it. Since the traverse mechanism is computer controlled, it makes it possible to move the ADV with precision, which is essential for the experiment.

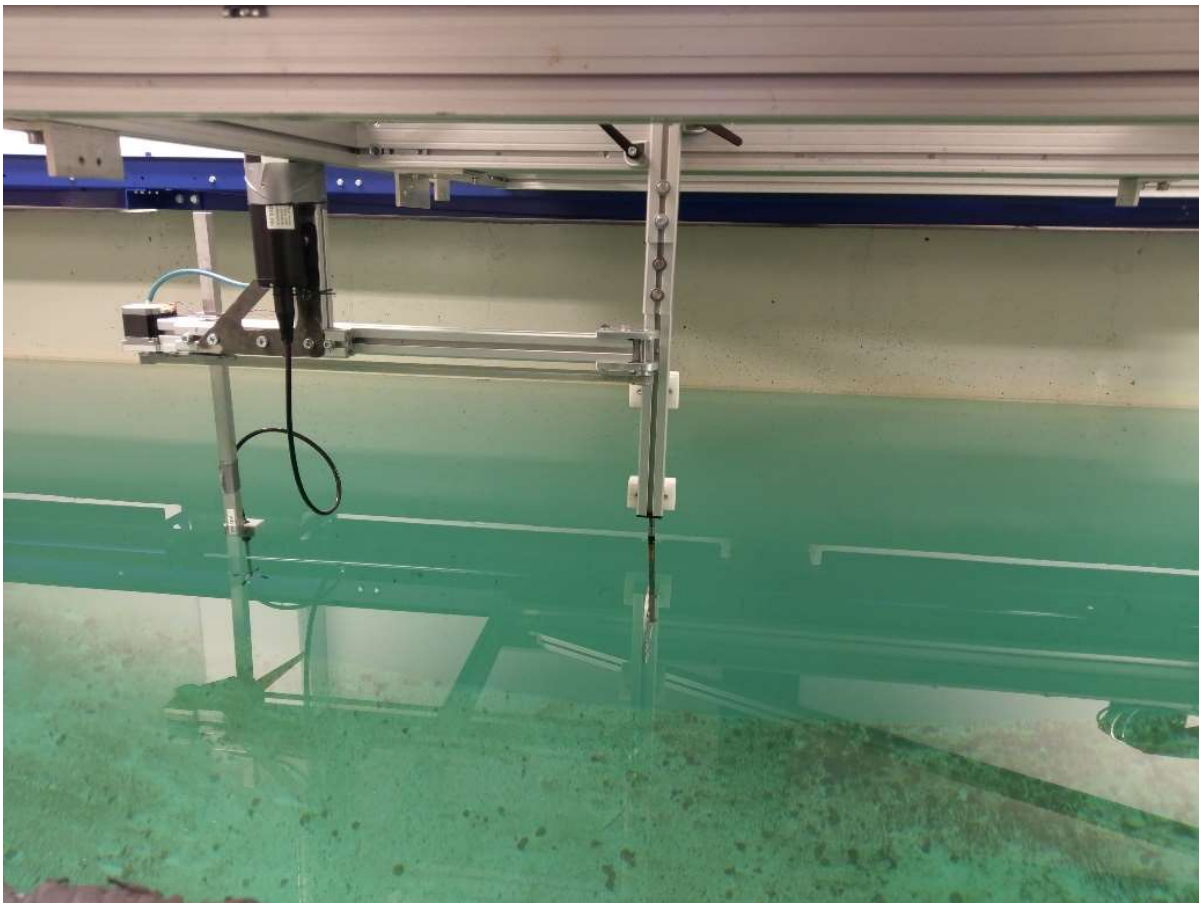

Figure 3.4 Picture of the experimental setup for up- and downstream centreline measurements. To the left one can see the traverse rig, with the attached ADV mounted to it. To the right one can see the Actuator Disc in the water.

3.2 Data Post-Processing

Simulations of wake and blockage has been used in a good amount of reports to examine different aspects of the phenomena. The computational method calculates idealized situations of the real world. To model a situation there is a process that consists of 3 phases: Pre-processing, Solving and Post-processing. One of the hurdles with computer models of the real world is the amount of details and accuracy. The vortexes that are created on a wind turbine blade can be a few milimeter wide while the blade itself is 200-meter-long. Simulating a whole park of wind turbines is not possible with the current processing power we have on computers today. The solution is to idealize and remove a lot of the phenomena happening at a micro scale.

The ADV measures and collects 200 points/s and thus collecting about 13000 points per measuring position. To plot all this data, the group was introduced to MatLab, which efficiently sorts the data. A main code was already prepared which simply calculates the mean- velocity and turbulent kinetic energy. When plotting the first wake profiles it became clear that some of the points deviated from the trend, mainly due to noise and smaller errors in the data recording. When inspecting a few selected points manually, it became clear that an acceleration effect and some noise interference were included in the recorded data, which manipulated the results.

In order to get rid of the acceleration effect, a script was made which would cut the timeseries, and thus simply remove the acceleration effect. For the noise-issues two types of filters were applied: a Hampel-filter to get rid of signal outliers, and a Low-pass filter to get rid of high-frequent noise in the signal. A few signal outliers occur because of non-present reflection of seeding particles caused by insufficient seeding. The Hampel filter identifies and replaces these signal outliers by calculating the median and the standard deviation based on the neighbouring signals. The low-pass filter only allows a certain amount of low frequency components to pass through and thus removing high-frequent noise.

4. Results

This chapter presents one dimensional wake profiles for a non-yawed disc at distances of 1D, 3D, 4D, 10D and -1D downstream of the disc, respectively. Whereas -1D naturally is upstream of the disc. Figure 4.1 shows the setup for measuring points. The red-dotted horizontal line represents the centreline measurements.

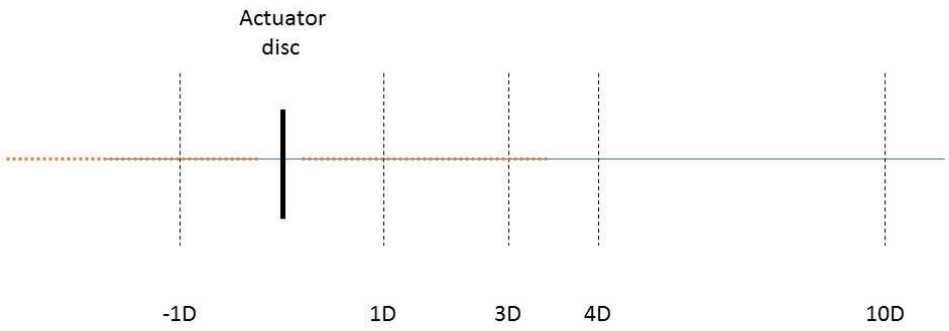

Figure 4.1 Schematics of the experimental measurement setup.

In order to visualize the results, the measured data was thoroughly analysed, sorted, and plotted in MatLab. Furthermore, a curve approximation is added to show the "trends" clearer. The dimensionless velocity U_{mean}/U_0 is obtained by dividing the local mean streamwise velocity by a reference velocity measured at a location outside of the wake effects. The turbulence intensity is defined as the ratio of standard deviation of fluctuating flow velocity to the mean flow speed, and it represents the intensity of the flow velocity fluctuation. [20]. The turbulence intensities are higher where velocities are higher and is derived from a reference value.

To study how the wake has developed with increasing distances from the disc, line wakes were measured from -1D to 10D. The evident development of the wake can be seen with an expansion of the wake as the downstream distance increases. The highest velocity deficit is found in the near-wake region, whereas the velocities increase with increasing distances due to turbulent mixing.

4.1 Wake Flow

The results from x=1D, x=3D and the upstream centreline is to be further discussed and compared to similar projects, in the discussion chapter.

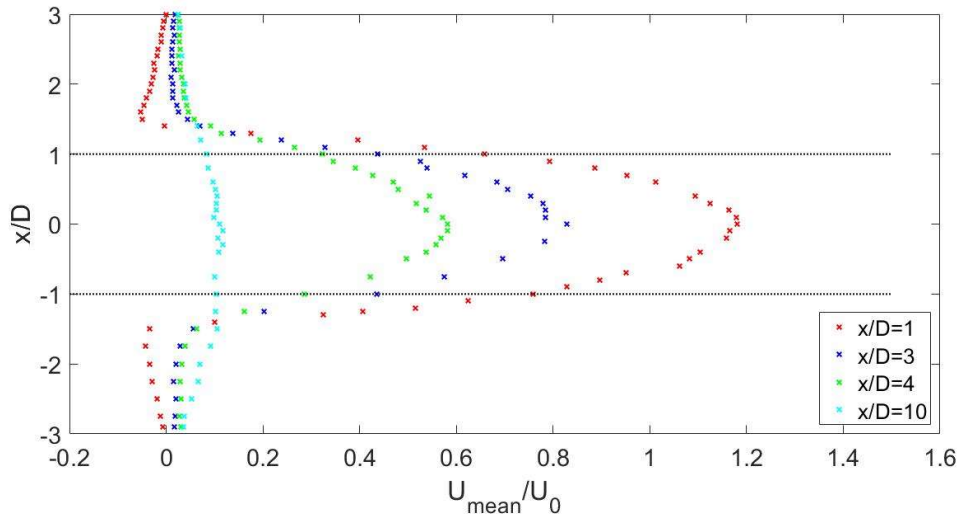

Figure 4.2 Profiles of the mean velocity at selected distances downstream of the non-yawed disc.

As expected, it shows a Gaussian-shaped wake deficit throughout the wake. At 1D the velocity deficit reaches a negative deficit of approximately 18%, in addition there is also a slight increase in velocity at about 1,5D on each side of the center. At 10D the velocity deficit has decreased to 11,65%.

4.1.1 Mean Velocity

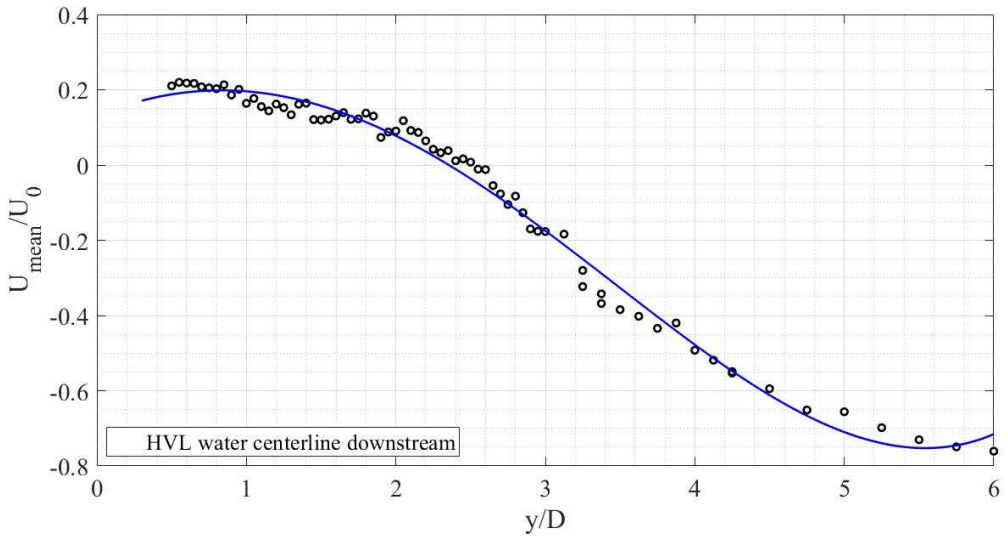

Figure 4.3 Mean velocity measured downstream.

At first, the results of the downstream centerline measurements are presented. The measurements presented in figure 4.3 were executed every 10'th mm from 0.5D to 6D and gives a good description of further expected results. The blue line represents a curve approximation. Notice the "upside-down" y-axis, meaning that $-1 = U_{mean} = U_0$.

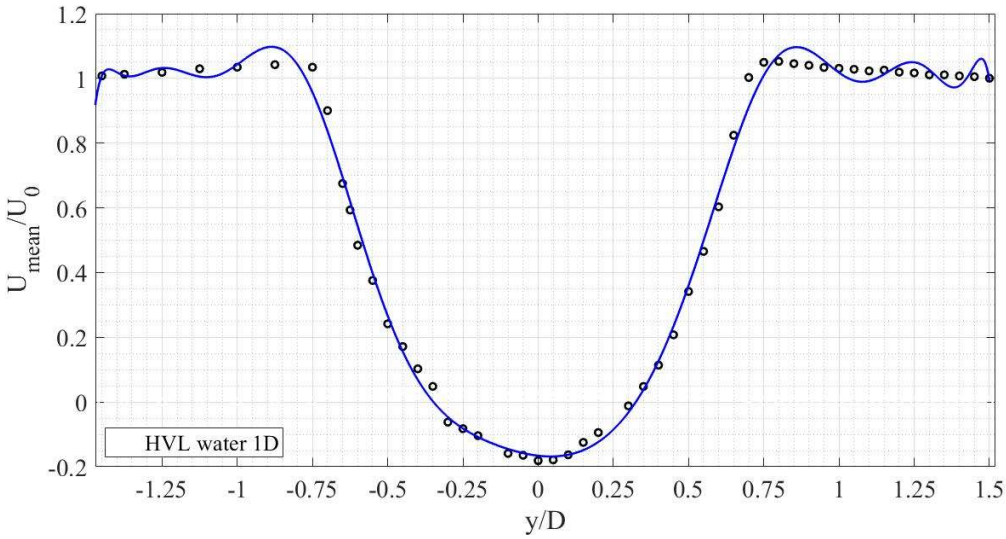

Figure 4.4 Mean velocity measured at x=1D downstream of the disc.

The first downstream wake-profile results to be presented is of the measurements of the near wake at 1D. Figure 4.4 shows the mean velocity profile measured in the wake. The wake flow at this very close downstream condition is clearly influenced by the geometry of the disc. Therefore, a high velocity deficit and turbulent kinetic energy is expected. The results show two distinct peaks at about 0.8D on each side of the disc. Here the velocity increases with an equivalent of 4,20% and 5,25% respectively (based on the measured points, not the curve). Also notice the graphs minima which reaches a negative velocity deficit of 18%. This flow-reversal zone will be further discussed in the next chapter.

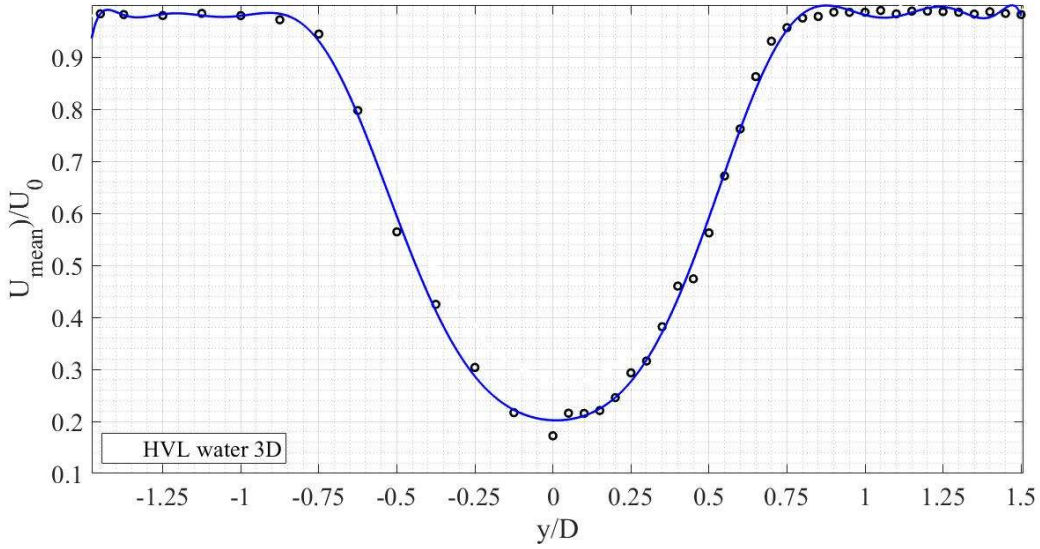

Figure 4.5 Mean velocity measured at x=3D downstream of the disc.

The second downstream distance to be presented is measurement results from x=3D. This can still be considered as the the near wake region, yet this is a turbine separation distance that occurs in very closely spaced wind farms e.g. Lillegrund windfarm in Denmark [21] . As expected, the results presented in figure 4.5 show that the wake have become a little wider, and there is no flow-reversal zone anymore. However, the wake still reaches a significant velocity deficit of 82,7% approximately (based on the measured points, not the curve).

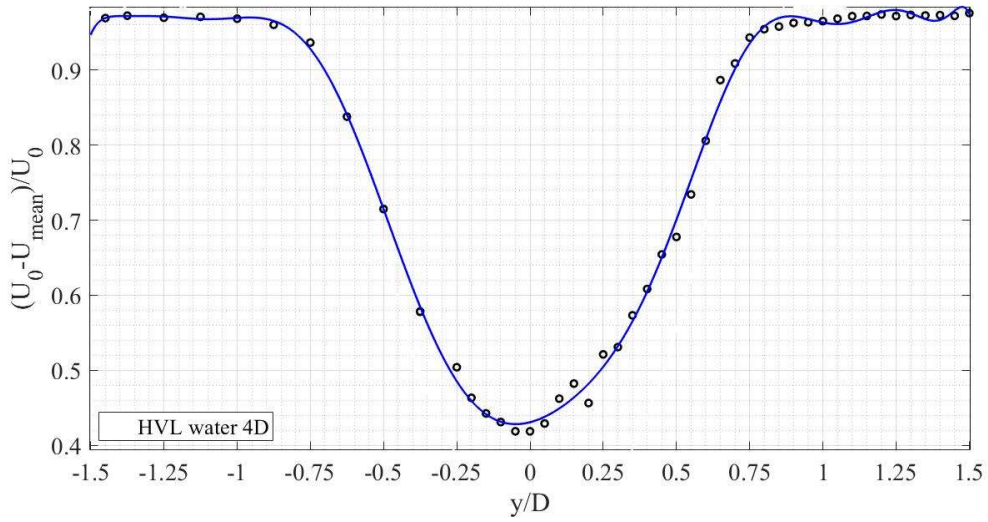

Figure 4.6 Mean velocity measured at x=4D downstream of the disc.

At only one rotor diameter further downstream, at x=4D the wake was measured to quantify the incremental changes in the wake within one diameters distance from y/D=3 to y/D=4. The results presented in figure 4.6 show a velocity deficit of approximately 58,1% (based on the measured points,

not the curve). Figure 4.6 also shows a minor drag of the wake's minima towards the negative end of the x-axis, which becomes more visual at the 10D results.

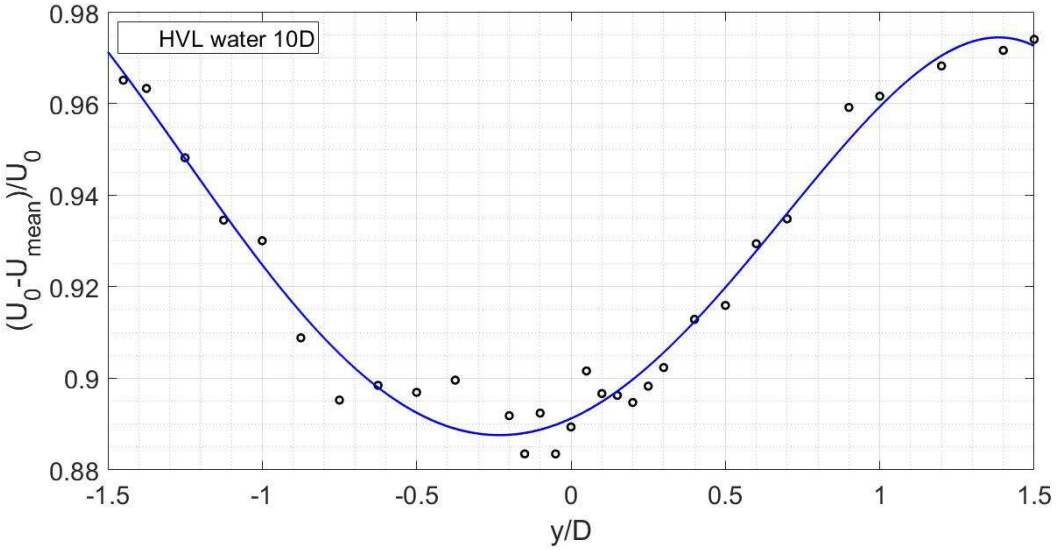

Figure 4.7 Mean velocity measured at x=10D downstream of the disc.

The last measured downstream distance at x=10, represents a recommended turbine spacing in the predominant wind direction [22]. The results presented in figure 4.7, shows a velocity deficit of approximately 11.65% (based on the measured points, not the curve). The drag most likely caused by a small yaw-angle, which became visuable at x=4D has now become more visuable and reaches towards y/D=0.25.

4.1.2 Turbulent Kinetic Energy

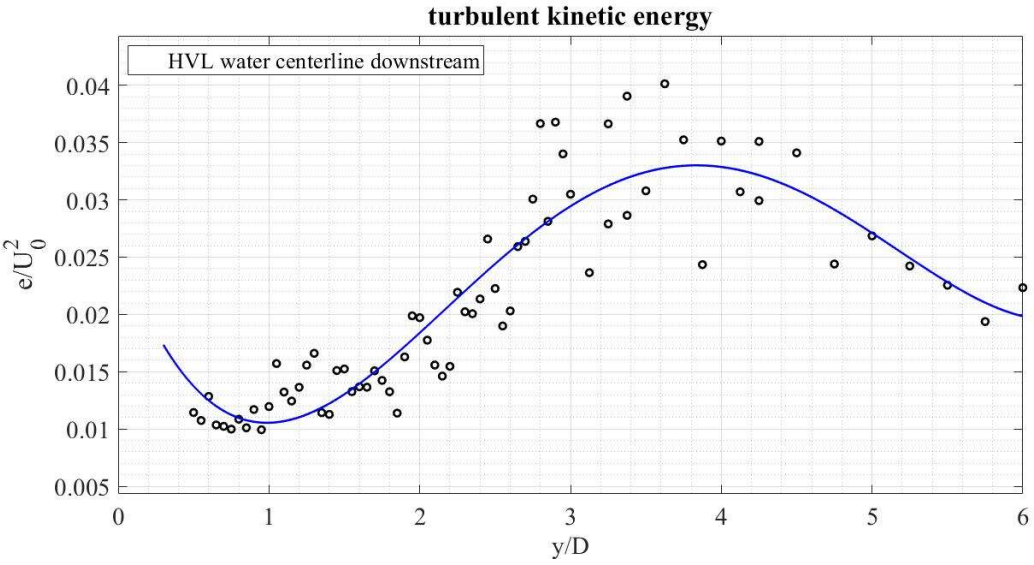

Figure 4.8 Turbulent kinetic energy measured downstream.

Figure 4.8 presents the results from the turbulent kinetic energy measured at the centreline downstream. Measurements were executed every 10'th mm, from y/D=0.5 to y/D=6. The results show a fluctuating sinus shape, and this shape also occurs in the upstream centreline measurements.

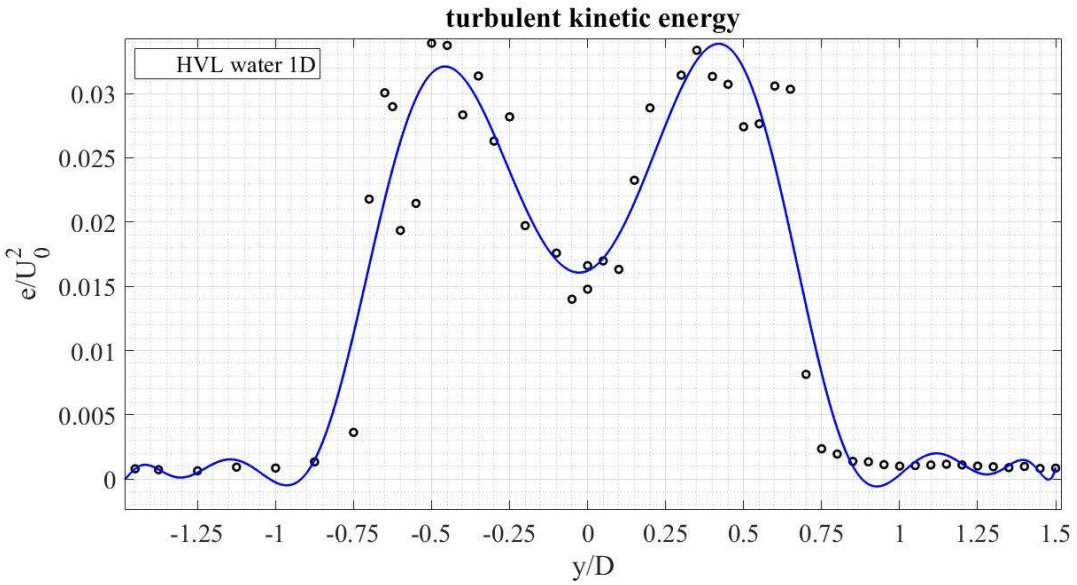

Figure 4.9 Turbulent kinetic energy measured at x=1D.

The first turbulent kinetic energy measurements downstream, at 1D is presented in figure 4.9. The result show that the turbulent kinetic energy is deflected to the same degree as the mean velocity profile. The results also present two distinct peaks, located at the edges of the disc at y/D=-0.5 and y/D=0.5. Watching the curve approximation, a slight asymmetry appears, which will increase further downstream.

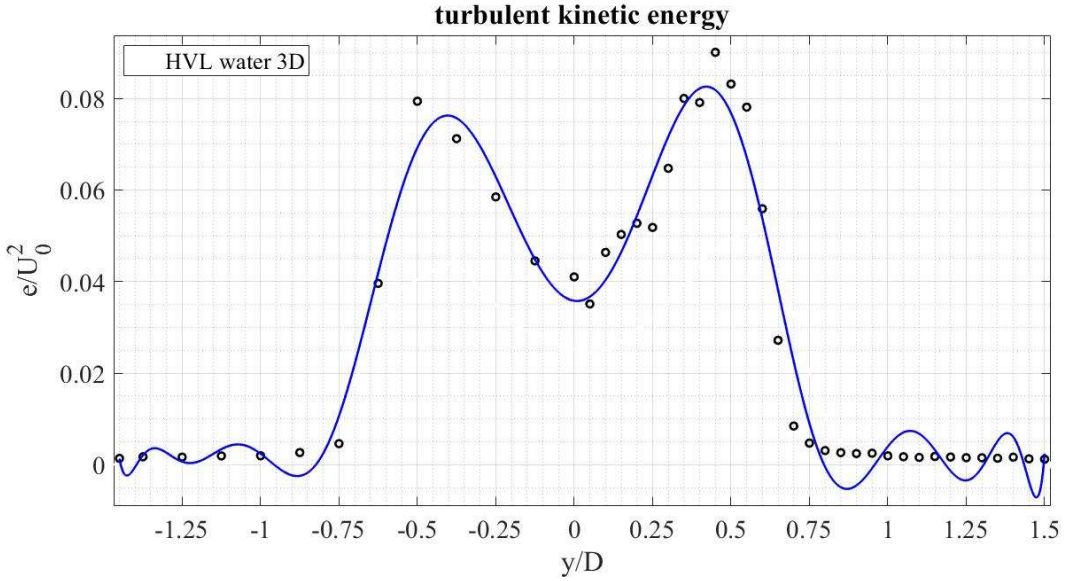

Figure 4.10 Turbulent kinetic energy measured at x=3D.

At 2D further downstream the results presented in figure 4.10, the asymmetry has become clearer. The two distinct peaks appear to be closing in towards the centre and is now located at y/D=-0.4 and y/D=0.4.

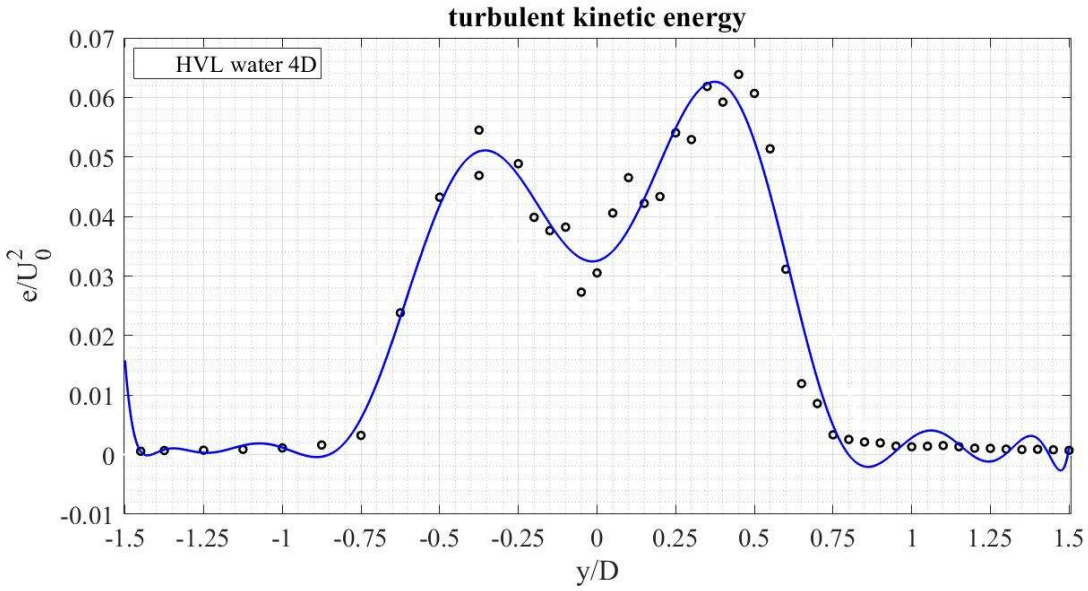

Figure 4.11 Turbulent kinetic energy measured at x=4D. Increasing asymmetry.

At only 1D further downstream, the trend from the two previous results has now become enhanced. The asymmetry has become very clear, and the peaks has moved even closer to the centre, and is now located y/D=-0.35 and y/D=0.35

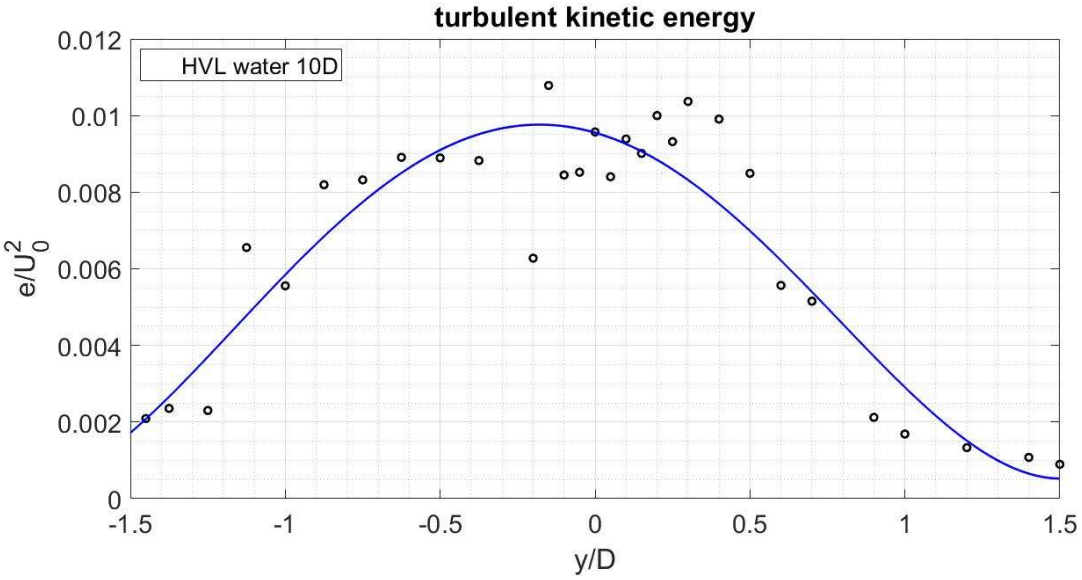

Figure 4.12 Turbulent kinetic energy measured at x=10D.

The results from the final measurement downstream, at 10D is presented in figure 4.12. These results, from the far-wake region show that the mixing of flow has eradicated the distinct peaks, and the wake appears to have expanded. Also, worth noticing, is the drag of the graps maximum, which corresponds with the mean velocity results presented in figure 19.

4.2 Upstream Blockage

4.2.1 Mean Velocity

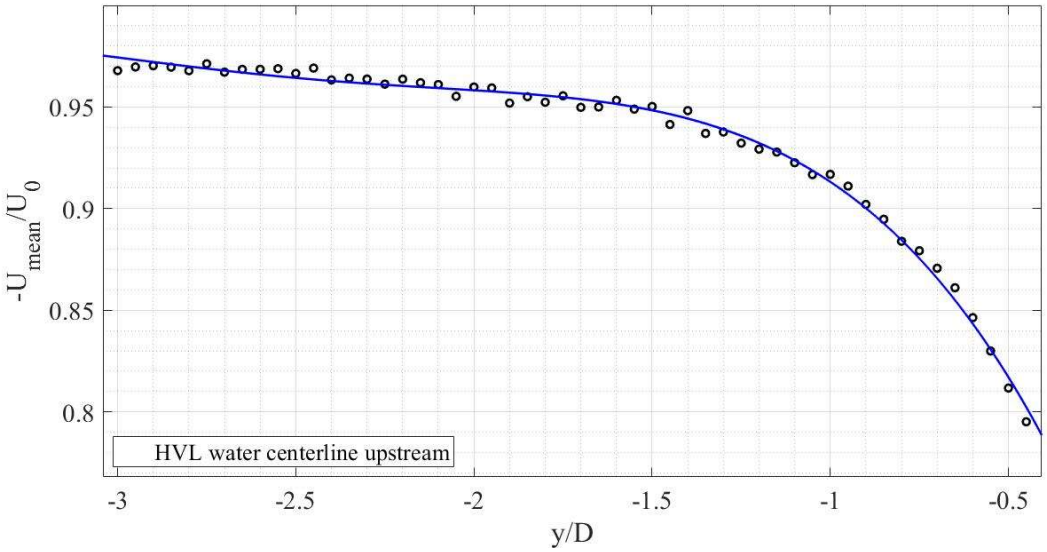

Figure 4.13 Mean velocity measured upstream.

The centerline measurements upstream represents a good visualization of the velocity deficit that is occurring as the flow reaches the rotor. Figure 25 shows that the measurements start three rotor diameters upstream, and a velocity reduction at approximately 20% upstream with an exponential shaped curve as the stream is reaching the rotor. Most of the velocity deficit occurs between two diameters upstream and the rotor.

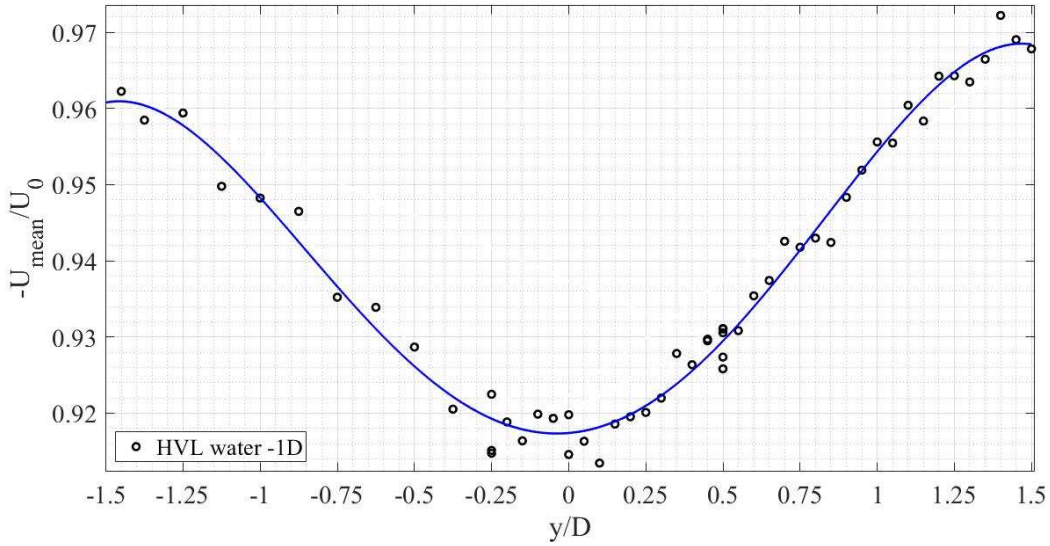

Figure 4.14 Mean velocity measured at x= -1D.

The mean velocity measured one diameter upstream of the rotor shows a velocity deficit of approximately 8.70% is represented based on the measured point. Again, an asymmetric curve can be observed. The wake flow velocity reduction close to the rotor upstream shows that the blockage effects has a relatively big impact and is very much present at this point. This effect is expected to increase as the flow approaches the rotor.

4.2.2 Turbulent Kinetic Energy

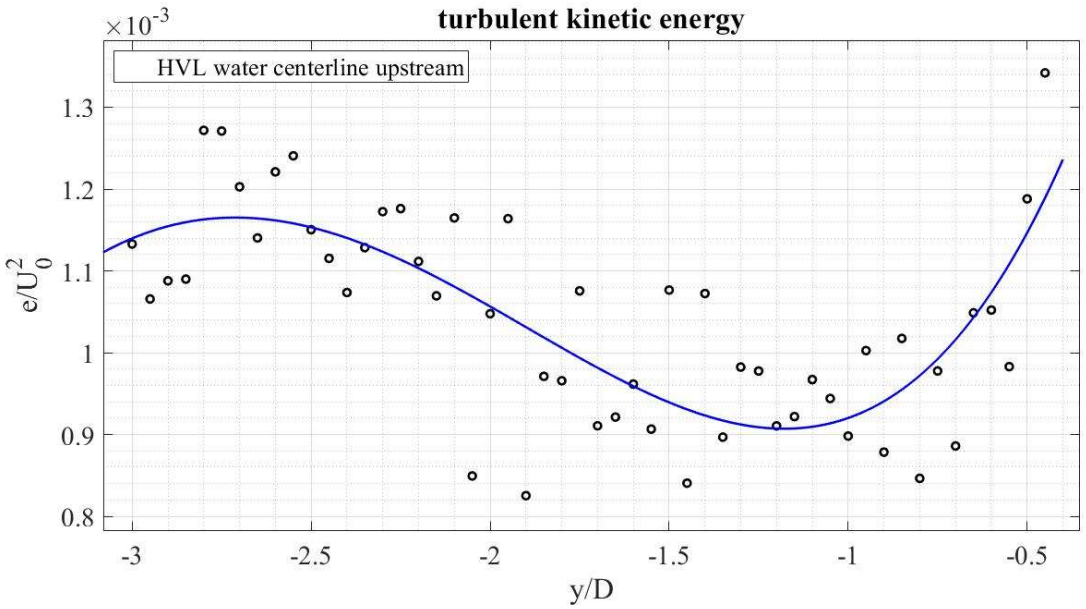

Figure 4.15 Turbulent kinetic energy measured upstream.

The centerline turbulent kinetic energy in figure 4.15 shows a sinus shape and represents a curve approximation. Measurements were executed every 10'th mm from y/D=-0.45 to y/D=-3.

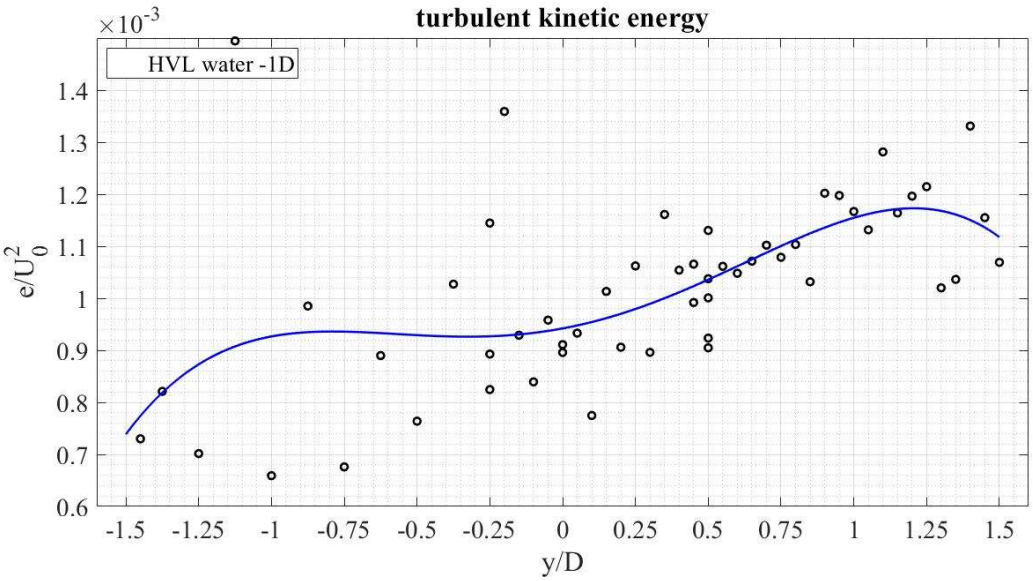

Figure 4.16 Turbulent kinetic energy measured at x=-1D.

The only measurement of the kinetic turbulence energy upstream at -1D is presented in figure 4.16. The results show that the characteristic peaks are present also in front of the disc, but the pattern is much more curved compared to the turbulence results downstream. The results show that there's only about 3.8% of the turbulent kinetic energy at -1D compared to the 1D measurements, making it practically non-existant.

5. Discussion

The velocity development of the experimental results represented in the previous chapter already suggests, that the measurements done in the Marin Lab seems to represent the wake profil of a wind turbine very well. The mean velocity profiles present a Gaussian-shape velocity deficit, due to the radially non-uniform porosity of the disc. The wake results at x = 3D are in the following compared to measurements behind the exact same disc at the wind tunnel at NTNU [23].

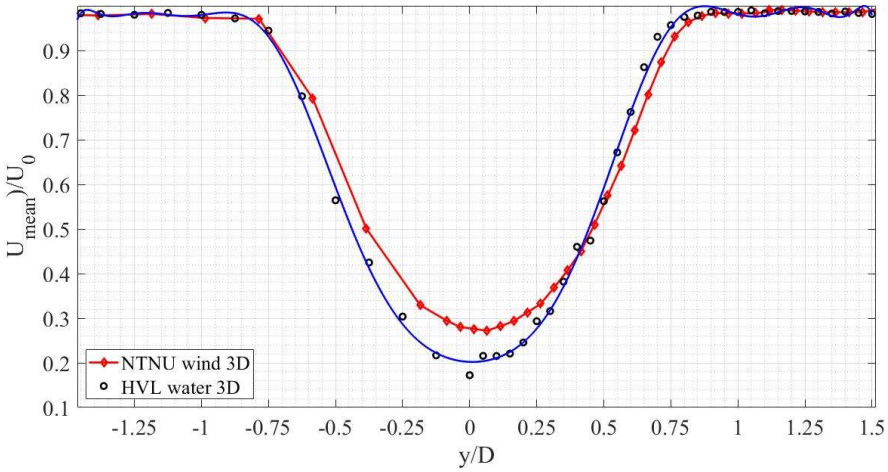

Figure 5.1 Mean velocity results compared to NTNU's results.

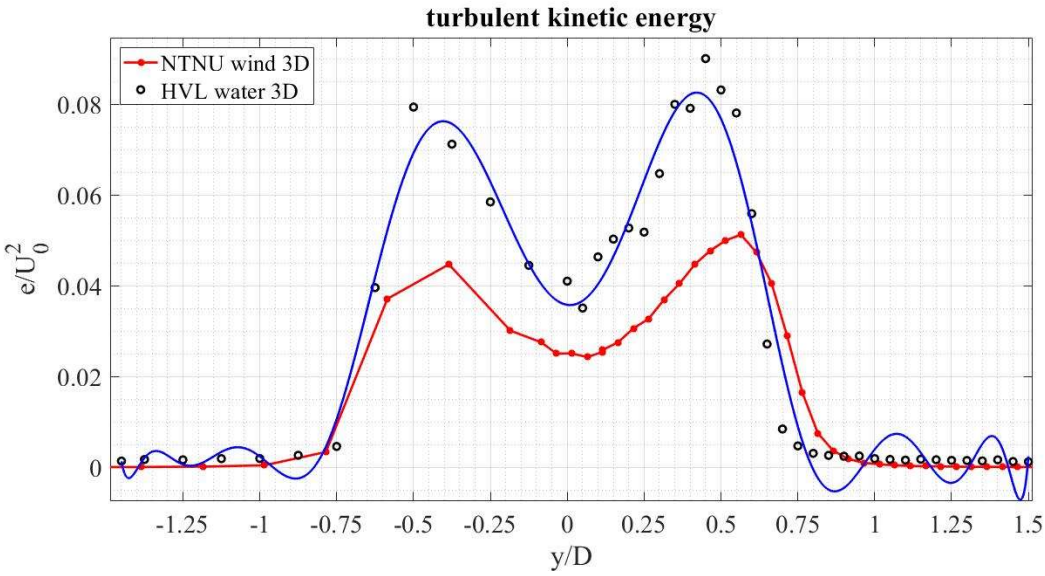

Figure 5.2 Turbulent kinetic energy results compared to NTNU's results.

However, due to measurement uncertainty a small random spread of the measurement points around the line can be observed. The turbulence intensity profiles present two maxima. In figure 29 the 3D velocity deficit profile from the experiment in the Marin Lab is compared with the test results from NTNU at 3D. On this first level of comparison, it can be concluded that the obtained results are consistent with each other, even if some slight discrepancies are visible. The profile from the Marin Lab experiment tends to have a lower minimum than the one from NTNU, and this is due to the fact that in the Marin Lab experiment there is low to nonturbulent inlet conditions.

In the measurements at 1D, a flow reversal zone is observed "around" the centreline. This corresponds with results presented by Marfort & Porte-Agel [24]. Their explanation suggests that this flow reversal is caused by the nacelle, the root vortices and a large pressure gradient induced by a strong near-wake rotation. However, since the experiment for this report were executed with a non-rotating actuator disc, it suggests that the flow reversal is mostly caused by a large pressure gradient.

In figure 5.3 the experiment mean velocity profiles is plotted and compared with the Jensen-Gauss model [25]. This is one of the newest wake models and is based on the original Jensen model using a Gaussian Wake shape. The model also takes ambient and rotor added turbulence into account. [23] Figure 5.3 shows that the Jensen-Gauss model is very sensitive to inputs as C_T and k, were k is the "wake-recovery factor" which is dependent on the turbulence intensity. The turbulence intensity is composed of "la" (atmospheric turbulence) and "I+" (wake added turbulence). In our experiment Ia ≈ 0, and according to Polster et al. the Jensen-Gauss model does not seem to be applicable with these conditions. Based on this comparison it confirms that the Jensen model is not applicable at low ambient turbulence intensities, and if the Ia > 10% the Jensen wake model performs significantly better [23]. For future wake experiments in the Marin Lab it would be recommended to have a grid generated turbulence at the inlet to make the results more comparable with other models. [25]

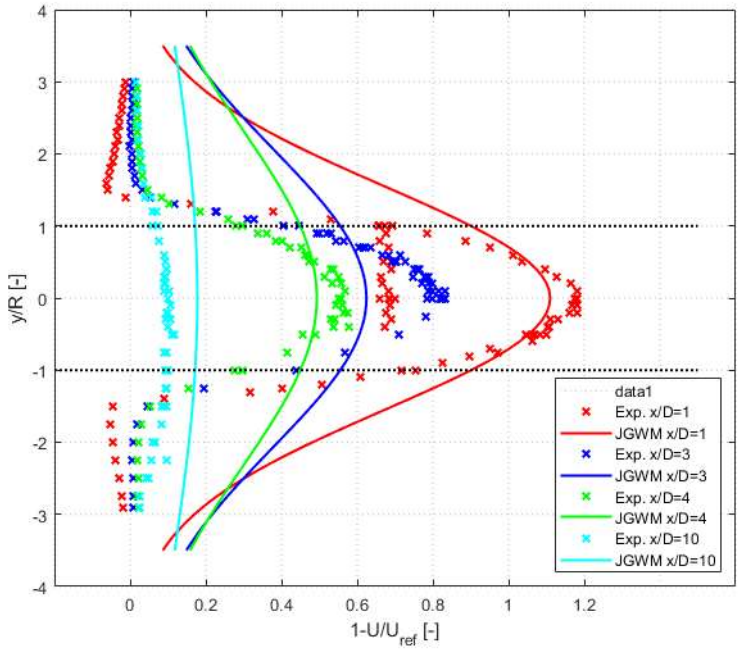

Figure 5.3 Experimental downstream results compared to the Jensen-Gauss model.

In figure 5.4 a comparison has been made between the experimental results from the upstream centreline measurements, and the Biot-Savart-Law with different thrust coefficient. Notice that the Biot-Savart graph with a Ct=0.82 (which is the same Ct as for the disc) is the one furthest away.

Whilst by using a Ct=1.15 is the closest to the experimental results. This means that for the disc used in this experiment, Biot-Savarts-law underestimates the velocity deficit, and Biot-Savart-law cannot be used directly as a comparison. However, for better quantification of the model's applicability it is recommended to use different discs with different porosity, and thus different Ct values.

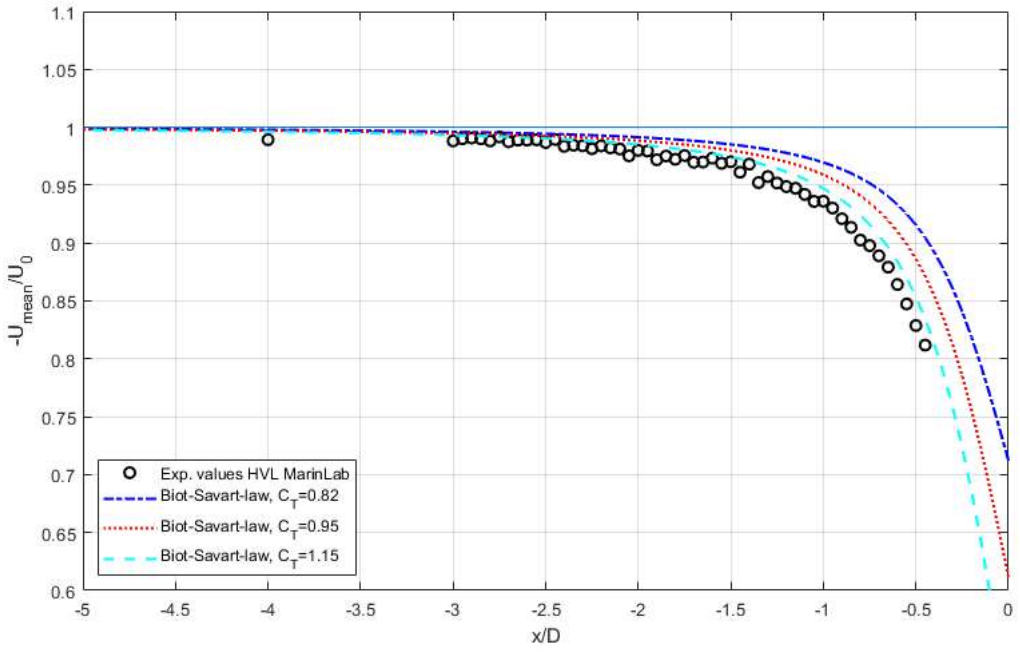

Figure 5.4 Comparison between Upstream centreline results and Biot-Savart-law.

6. Conclusions

A wake-and blockage effect experiment on an actuator disc representing a wind turbine rotor has been performed in the Marin Lab at Western University of Applied Science. Point measurements have been done at different centerline and cross-sectional positions downstream and upstream of the disc with an Acoustic Doppler Velocimiter (ADV). Four high resolution traverse wake profiles were measured to quantify the flow in the horizontal plane covering a streamwise range from 1 rotor diameter upstream of the disc to 10 diameters downstream. The test results of the velocity deficit were compared with previous measurements done in a wind tunnel and the mean values showed a good overlap with the results. Also, the expected Gaussian shape of the velocity deficit in the far wake regime of a disc in water was observed by the experiment setup. The wake results have been compared with Jensen-Gauss model and it shows that the model underestimates the wake that suggest that Jensen-Gauss is not suitable with zero inlet turbulence. The measured results on the centerline velocity deficit shows that at 3D downstream the velocity is 20% of the reference velocity V_0 and at 4D its 50% recovered to the V_0, its also clear that it is a linear velocity deficit in the range from 2D to 5D downstream. Comparing the velocity reduction due to upstream blockage with predictions given by the Biot-Savart-Law *I* the measured velocity deficit is larger than what is predicted by the law for the given thrust coefficient, meaning that the law underestimates the velocity deficit in front of the disc. Exploring the causes of this mismatch between the experiment and the Biot-Savart-Law *I* above demand more testing with several disc with different porosities and thrust coefficients.

Test results from the Marin Lab shows a slightly higher velocity deficit and turbulence intensity compared to wind tunnel results from NTNU and the other wake/blockage models mentioned in this report. But this is concluded mainly to be caused due to difference in inlet turbulence. However, these results show the ability of the equipment in the Marin Lab to accurately measure wake behaviors of a wind turbine in a satisfying manner, and the experimental method used in this report can be of good value for further work on exploring wake effects in wind farms at the Marin Lab at HVL in the future.

7. Referances

[1] B. ,. S. Portè-Agel, "Wind-Turbine and Wind-Farm Flows: A Review," *Boundary-Layer Meteorology,* p. 54, 17 October 2018.

[2] S. Karlsen, "Cross-sectional wake measurements of Actuator disks.," Department of Energy and Process Engineering, NTNU, Trondheim, 2011.

[3] D. G. Berghäll, "Wind-Farm-Scale Blockage Effects: Points of Clarification.," *Energies,* p. 20, 2019.

[4] M. O. Hansen, Aerodynamics of Wind Turbines, London: Earthscan, 2008.

[5] R. K. Bhargava, "Axial induction factor & Pressure distribution on wind turbine blades," GITAM University, Hyderabad , 2019.

[6] S. P. A. D. Medici, "The upstream flow of a wind turbine: blockage effect," Wiley Online Library, 2011.

[7] I. N. N. I. K. R. M. a. J. N. S. V L Okulov, "Experimental investigation of the wake behind," IOP Publishing, 2014.

[8] M. B. a. S. S. Fernando Porté-Angel, "Wind-Turbine and Wind-Farm Flows: A Review," Boundary-Layer Meteorology, 2019.

[9] L. Y. a. L. Gao, "Comparison and validation of wake models based on field measurements with lidar," University of Beijing , Beijing, 2018.

[10] L. Tian, W. J. Zhu, W. Z. Shen, N. Zhao and Z. Shen, "Development and validation of a new two-dimensional wake model for wind turbine," Journal of Wind Engineering and Industial Aerodynamics, 2015.

[11] T. Gögmen, P. van der Laan, P.-E. Réthoré, A. Pena Diaz and G. C. Larsen, "Wind turbine wake models developed at the Technical University of Denmark: A review," Renewable & sustainable Energy Reviews, 2016.

[12] C. G. A. P. CUMMINS, "The efficiency of a turbine in a tidal channel," Cambridge University, Cambridge, 2007.

[13] T. N. a. S. Draper, "Local blockage effect for wind turbines," IOP Publishing, 2015.

[14] M. P. R. R. a. E. T. James Bleeg, "Wind Farm Blockage and the Consequences of Neglecting Its Impact on Energy Production," DNV GL, 2018.

[15] T. N. a. R. H. J. Willden, "The efficiency of an array of tidal turbines," Fluid Mech., 2012.

[16] N. R. M. a. J. N. S. Okulov, "Experimental investigation of the wake behind a model of wind turbine in a water flume," Publishing Ltd, Oldenburg, 2012.

[17] S. Steen, Experimental Methods in Marine Hydrodynamics, Trondheim: Marine Technology Centre, 2014.

[18] E. Toolbox, "https://www.engineeringtoolbox.com/," Engineering Toolbox, [Online]. Available: https://www.engineeringtoolbox.com/reynolds-number-d_237.html. [Accessed Thursday April 2020].

[19] Nortek AS, "Nortekmed," [Online]. Available: http://www.nortekmed.com/images-repository-1/vectrino/DownLooking.jpg/view. [Accessed April 2020].

[20] L.-Z. Zhang, "Turbulence Intensity," *Innovative Bridge Design Handbook,* p. 1, 2016.

[21] A. F. W.-G. &. M. A. E. Creech, "A. Eoghan Maguire," Springer Science+Business Media Dordrecht , Dordrecht , 2014.

[22] I. Mustakerov and D. Borissova, "Wind Park Layout Design Using Combinatorial Optimization," Institute of Information and Communication Technologies of Bulgarian Academy of Sciences , 2011.

[23] B. M. T. &. S. Polster, "Experimental validation of amalytical wake and downstream turbine performance modelling," NTNU, Trondheim, 2018.

[24] C. D. M. &. F. P.-A. Wei Zhang, "Near-wake flow structure downwind of a wind turbine," Springer -Verlag, 2011.

[25] Y. L. Gao, "Optimization of wind turbine layout positon in a wind farm using a newly-developed two-demensional wake model," The Hong Kong Polytechnic University, Hong Kong, 2016.

[26] B. Szabo and I. Babuska, Finite Element Analysis, Wiley & Sons, Inc., 1991.

[27] K. J. Rawson and E. C. Tupper, Basic Ship Theory, 5 ed., Jordan Hill, Oxford and Woburn, MA: Elsevier Butterworth-Heinemann, 2001, p. 91.

[28] K. Garme and A. Rosén, "Time-domain simulation and full-scale trials on planing craft in waves," *International Shipbuilding Progress,* vol. 50, pp. 177-208, 2006.

[29] K. Garme and A. Rosén, "Experimental pressure investigation on high-speed craft in waves," in *International Conference on Hydrodynamicd of High-Speed Craft*, RINA, UK, 2000.

[30] A. Keller, *Loads and responses for planing craft in waves,* 2004.

[31] NASA Langley Research Center, January 2012. [Online]. Available: http://www.nasa.gov/vision/earth/improvingflight/x48b.html.

[32] The MathWorks, Inc., *Matlab - Primer R2013b,* Natick, 2013.

[33] M. V. F. M. a. L. S. Luis García, "Experiments in the wind turbine far wake for the evaluation of an analytical wake model," IOP Publishing, 2017.

[34] Y.-T. W. &. F. Porté-Agel, "Large-Eddy Simulation of Wind-Turbine Wakes," 2010.

[35] A. Berghäll, "DNV GL," DNV GL, 08 11 2019. [Online]. Available: https://www.dnvgl.com/news/wind-farm-scale-blockage-effects-points-of-clarification-161311. [Accessed 15 02 2020].

[36] nortekgroup, [Online]. Available: https://www.nortekgroup.com/products/vectrino. [Accessed 02 2020].

[37] L. Li, Y. Cui, Y. Liu, L. Gao, N. Wang and H. Lei, "Comparison and validation of wake models based on field measurements with lidar," IET, London, 2016.

[38] A. H. Tambaani, "Groundschoolacademy," [Online]. Available: http://groundschoolacademy.blogspot.com/2017/02/principles-of-flight-aerodynamics-iii.html. [Accessed 12 04 2020].

[39] M. B. &. S. S. Fernando Porté-Agel, "Springer Link," 2020. [Online]. Available: https://link.springer.com/article/10.1007/s10546-019-00473-0. [Accessed 01 05 2020].

List of figures